






# 32QAM WDM transmission at 12 Tbit/s using a quantum-dash mode-locked laser diode (QD-MLLD) with external-cavity feedback

JUNED N. KEMAL,<sup>1</sup>  PABLO MARIN-PALOMO,<sup>1</sup>  KAMEL MERGHEM,<sup>2,3</sup> GUY AUBIN,<sup>2</sup> FRANÇOIS LELARGE,<sup>4</sup> ABDERRAHIM RAMDANE,<sup>2</sup> SEBASTIAN RANDEL,<sup>1</sup> WOLFGANG FREUDE,<sup>1</sup>  AND CHRISTIAN KOOS<sup>1,5,\*</sup> 

<sup>1</sup>*Institute of Photonics and Quantum Electronics (IPQ), Karlsruhe Institute of Technology (KIT), Germany*

<sup>2</sup>*Centre de Nanosciences et de Nanotechnologies (CNRS), Univ. Paris-Sud, C2N - Université Paris-Saclay, France*

<sup>3</sup>*Now with Institut Mines-Télécom - Télécom SudParis, EVRY, France*

<sup>4</sup>*Now with Almae Technologies, Marcoussis, France*

<sup>5</sup>*Institute of Microstructure Technology (IMT), Karlsruhe Institute of Technology (KIT), Germany*

\*[christian.koos@kit.edu](mailto:christian.koos@kit.edu)

**Abstract:** Chip-scale frequency comb generators lend themselves as multi-wavelength light sources in highly scalable wavelength-division multiplexing (WDM) transmitters and coherent receivers. Among different options, quantum-dash (QD) mode-locked laser diodes (MLLD) stand out due to their compactness and simple operation along with the ability to provide a flat and broadband comb spectrum with dozens of equally spaced optical tones. However, the devices suffer from strong phase noise, which impairs transmission performance of coherent links, in particular when higher-order modulation formats are to be used. Here we exploit coherent feedback from an external cavity to drastically reduce the phase noise of QD-MLLD tones, thereby greatly improving the transmission performance. In our experiments, we demonstrate 32QAM WDM transmission on 60 carriers derived from a single QD-MLLD, leading to an aggregate line rate (net data rate) of 12 Tbit/s (11.215 Tbit/s) at a net spectral efficiency (SE) of 7.5 bit/s/Hz. To the best of our knowledge, this is the first time that a QD-MLLD optical frequency comb has been used to transmit an optical 32QAM signal. Based on our experimental findings, we perform simulations that show that feedback-stabilized QD-MLLD should also support 64QAM transmission with a performance close to the theoretical optimum across a wide range of technically relevant symbol rates.

© 2020 Optical Society of America under the terms of the [OSA Open Access Publishing Agreement](#)

## 1. Introduction

With escalating data traffic on all levels of optical communication networks [1], wavelength-division multiplexing (WDM) is becoming a necessity not only for long-haul links, but also for shorter transmission distances of a few tens of kilometers as typically found in data-center interconnects and in metropolitan or campus-area networks. To provide utmost scalability, these links should rely on compact WDM transceivers that can be efficiently produced in large quantities and that offer multi-terabit/s connectivity. In this context, chip-scale frequency comb generators have emerged as promising building blocks of WDM transceivers [2,3], acting either as multi-wavelength light source for massively parallel data transmission [4–10] or as multi-wavelength local oscillator (LO) for coherent reception [4,11–14]. Among different comb generator concepts that have been used for WDM transmission at Tbit/s data rates and that relied, e.g., on electro-optic modulators [8,9], gain-switched laser diodes [7,13], Kerr-nonlinear waveguides [6] or micro-resonators [4,5], quantum-dash mode-locked lasers (QD-MLLD) [10,15,16] are a particularly

attractive option due to their compact size and operational simplicity. Driven by a DC current, a QD-MLLD can emit a broadband comb containing tens of evenly spaced tones with a flat spectral envelope [17,18]. However, while the power and the optical carrier-to-noise ratio (OCNR) of QD-MLLD would permit high-speed communication using advanced modulation formats [2,16,19], the devices suffer from large optical linewidths of the individual tones, which strongly impairs transmission of signals that rely on advanced modulation formats. As a consequence, previous demonstrations of WDM transmission with native QD-MLLD had to rely on intensity modulation of the optical carriers [20,21], were limited to rather simple modulation formats such as quadrature phase-shift keying (QPSK) [10,14], or required advanced phase tracking schemes to permit 16-state quadrature amplitude modulation (16QAM) transmission [16].

In this paper, we show that QD-MLLD can support WDM transmission with modulation formats beyond 16QAM if external-cavity optical feedback is used to reduce the phase noise [22]. In our experiments, we demonstrate a reduction of the intrinsic linewidth by approximately two orders of magnitude, and we use the devices to demonstrate 32QAM WDM transmission at a symbol rate of 20 GBd, limited by the free spectral range (FSR) of the comb generator. We transmit 60 channels derived from a single comb source over a 75 km-long standard single mode fiber (SSMF). Using two polarizations, we achieve an aggregate line rate (net data rate) of 12 Tbit/s (11.215 Tbit/s) at a net spectral efficiency (SE) of 7.5 bit/s/Hz. To the best of our knowledge, this is the first time that a QD-MLLD optical frequency comb has been used with 32QAM signaling, leading to the highest spectral efficiency reported for such a device. Our experiments complement recent WDM demonstrations that exploit feedback-stabilized quantum-dot MLLD for 16QAM signaling at comparable data rates [23]. Combining our results with recently demonstrated integrated optical feedback circuits based on ring resonators [24] opens a route towards chip-scale WDM transceivers supporting line rates of tens of Tbit/s.

## 2. QD-MLLD comb sources and external feedback

The basic structure of the QD-MLLD used in this work is depicted in Fig. 1(a). The devices comprise an active region made from three separate layers of InAs quantum dashes (QD) grown by molecular beam epitaxy on an InP substrate. The InAs QD layers are separated by 40 nm-thick InGaAsP barriers using a dash-in-a-barrier design [17]. The dash-barrier stack is terminated at the top and the bottom by 80 nm-thick InGaAsP separate confinement heterostructure (SCH) layers. The optical mode is guided by a buried-ridge waveguide, having a width of 1.0  $\mu\text{m}$  and a length of 1.71 mm, which is formed by the dash-barrier stack. Cleaved chip facets form a Fabry-Perot laser cavity having a free spectral range of approximately 25 GHz. Light is emitted from both facets. The active region of the QD-MLLD is electrically pumped via p-doped and n-doped InP layers using top and bottom contact pads. Proton ( $\text{H}^+$ ) implantation ensures lateral confinement of the pump current [17]. Shape and size variations of the QD result in an inhomogeneous broadening of the gain spectrum, which leads to multiple longitudinal modes oscillating simultaneously with nearly the same strength [25]. Nonlinear interaction of these longitudinal modes results in mode-locking, characterized by equidistant optical tones with strongly correlated phase noise [26].

It has been shown both theoretically and experimentally that coupling a properly adjusted external resonator to a passively mode-locked semiconductor laser leads to a reduction of the optical linewidth [27–31], and this concept was also transferred to QD-MLLD [32,33]. In this work, we rely on a free-space optical feedback, see Fig. 1(b) for a sketch of the experimental setup. The output light of the laser diode enters an external cavity formed by the cleaved facet and a highly reflecting plane metallic mirror, placed 30 cm away from the chip facet. A plano-convex lens collimates the beam emitted from the laser, and a variable attenuator is used to adjust the quality factor of the cavity, thereby adapting the level of optical feedback to avoid unstable operation [30–32]. The mirror position is manually adjusted such that the cavity length

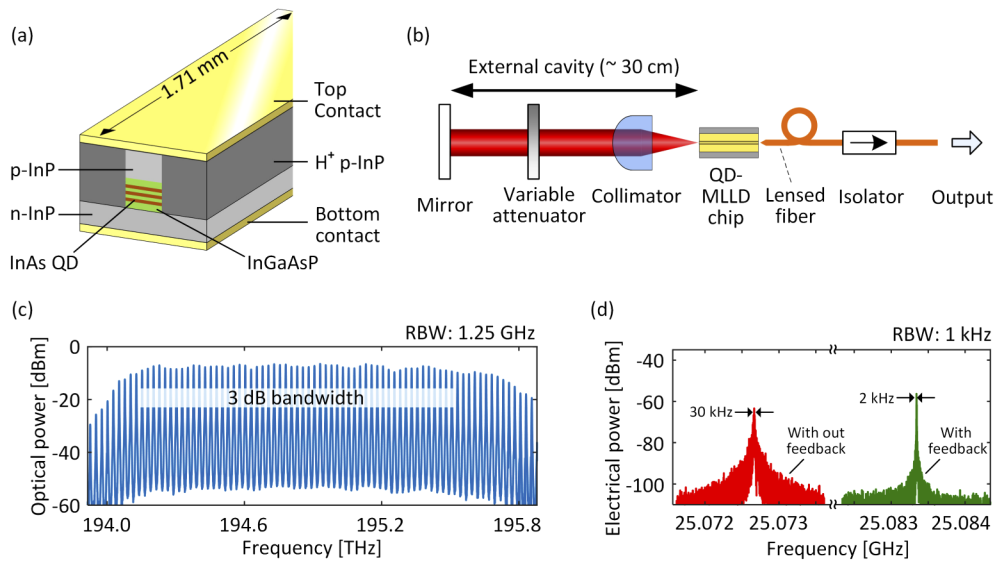


**Fig. 1.** Quantum-dash mode-locked laser diode (QD-MLLD) with optical feedback from an external cavity. (a) Schematic of a QD-MLLD: The device consists of stacked layers of InAs quantum dashes (QD, red) that are separated by InGaAsP barriers (green). Separate confinement heterostructure (SCH) InGaAsP layers terminate the dash-barrier stack at the top and the bottom. The optical mode is guided by a dash-barrier stack acting as a buried ridge waveguide of  $1.0\ \mu\text{m}$  width. Cleaved chip facets form a Fabry-Perot laser cavity having a length of  $1.71\ \text{mm}$ , thus leading to a free spectral range (FSR) of about  $25\ \text{GHz}$ . The active region of the QD-MLLD is electrically pumped via p-doped and n-doped InP layers using top and bottom contact pads. Proton ( $\text{H}^+$ ) implantation ensures lateral confinement of the pump current. (b) Optical setup for external feedback: An anti-reflection-coated collimating lens collimates the output light of the laser diode and directs it to a highly reflecting external mirror, which forms a Fabry-Perot cavity together with the cleaved laser facet. The mirror position can be mechanically adjusted to match the FSR of the external Fabry-Perot cavity to an integer fraction of the native FR of the QD-MLLD. A variable attenuator in the external cavity allows to adjust the power level of the optical feedback. The attenuator is necessary to avoid excessive feedback, which could lead to unstable operation of the QD-MLLD [30–32]. (c) Optical comb spectrum of the QD-MLLD with optical feedback. RBW: resolution bandwidth. (d) Measured RF spectrum of the photo-mixed comb lines without (red) and with (green) optical feedback. The RF linewidth reduces from  $30\ \text{kHz}$  for a free-running QD-MLLD to approximately  $2\ \text{kHz}$  once the external-cavity feedback level is properly adjusted. At the same time, a slight spectral shift can be observed once the comb is locked to the external cavity.

is close to an integer multiple of the effective optical length of the Fabry-Perot laser cavity. In our case, the chip FSR equals 50 times the external-cavity FSR. The adjustment of the cavity mirror is reasonably stable and only needs some minor tuning from time to time to compensate for temperature drift of our experimental setup. During our data transmission experiments, which took many hours, we typically needed to re-adjust the cavity mirror position every 2-3 hours. The variable attenuator was left untouched in all cases. In real-world systems based on integrated optical feedback circuits [24], such adjustments might either be unnecessary or can be accomplished using a simple control loop. The light emitted from the second facet of the QD-MLLD enters a lensed fiber and a subsequent isolator. Figure 1(c) depicts the frequency comb spectrum obtained at the isolator output for a drive current of  $312\ \text{mA}$ . The comb is centered

at 1545 nm and exhibits a 3 dB bandwidth of more than 1 THz. The comb lines exhibit optical carrier-to-noise power ratios (OCNR) in the range of 36 . . . 38 dB, specified with respect to a reference noise bandwidth of 0.1 nm. Unlike single-line or dual-line injection locking [34,35], which lead to pronounced spectral variations of the comb tone powers, a simultaneous feedback for all lines qualitatively preserves the flat and broadband spectral envelope of the native comb [33,36]. However, as discussed in [36,37], a slight reduction of the overall comb bandwidth could occur, depending on the feedback conditions. In addition, a small spectral red shift of the whole comb spectrum is observed, which we attribute to a decrease in threshold carrier density due to a slight reduction of the laser cavity mirror losses with coherent feedback [38]. As a quickly accessible experimental indicator for adjusting the external-cavity feedback, we use the electric radio-frequency (RF) spectrum of the photocurrent obtained by detecting the comb on a high-speed photodiode. We consider the linewidth of the first harmonic of the photocurrent, occurring at the FSR frequency of approximately 25 GHz, see Fig. 1(d). This so-called RF linewidth of the comb [39] reduced from 30 kHz for a free-running QD-MLLD to approximately 2 kHz once the external-cavity feedback level is properly adjusted. A reduced RF linewidth indicates an improved overall coherence of the comb tones and hence a better mode-locking [40,41]. At the same time, a slight spectral shift of the RF beat note can be observed once the comb is locked to the external cavity, which amounts to approximately 10 MHz in the example shown in Fig. We attribute this shift to the fact that the FSR of the native comb is not an integer multiple of the external-cavity FSR [27].

Note that the RF linewidth only represents the relative phase noise of neighboring comb lines. It is not an indicator of the optical linewidth of the individual optical tones and that is relevant for the transmission performance. To characterize the phase noise of the individual optical carriers, we use the setup shown in Fig. 2(a) and we follow the technique described in Refs. [16,42,43] to extract the frequency-noise spectrum  $S_{f_i}(f)$  of different comb tones without and with external-cavity feedback. A tunable band-pass filter (TBF) is used to select a tone from the frequency comb. This tone is sent through a polarization controller (PC) and then superimposed with a local oscillator (LO) laser in a 90° optical hybrid. The LO is a high-quality external-cavity laser (ECL, Keysight N7714) with an intrinsic optical linewidth smaller than 10 kHz. At the output of the optical hybrid, balanced photodetectors (BPD) followed by an 80 GSa/s real-time oscilloscope (RTO) are used to capture the in-phase (I) and the quadrature (Q) component of the beat signal. The duration of the recorded signal window was 200 μs. The beat signal is centered on an intermediate frequency (IF) of 2 GHz defined by the detuning of the LO and the comb tone of interest. We then extract the time-dependent phase of the complex beat signal and remove the intermediate frequency by fitting a linear function to the unwrapped measured phases and by subtracting the fitted function to remove the slope. This leads to the time-dependent phase fluctuations  $\phi(t)$ , from which the instantaneous optical frequency  $f_i(t)$  is calculated by means of a differentiation,

$$f_i(t) = \frac{1}{2\pi} \frac{d\phi(t)}{dt} \approx \frac{1}{2\pi} \frac{\phi(t + \tau) - \phi(t)}{\tau}. \quad (1)$$

In this relation, the time step  $\tau$  corresponds to the sampling period of the RTO. The spectrum  $S_{f_i}(f)$  is then calculated by taking the Fourier transform of the autocorrelation function of  $f_i(t)$ .

Generally, the frequency noise spectrum  $S_{f_i}(f)$  of a laser is composed of flicker frequency noise ( $\propto f^{-1}$ ), random-walk frequency noise ( $\propto f^{-2}$ ), and a spectrally constant “white” frequency noise. If, as in our setup, the measured phase of the laser is additionally impacted by additive white Gaussian noise (AWGN) caused by, e.g., the ASE of an optical amplifier in the measurement setup, the frequency noise spectrum will also have a component with an  $f^2$ -dependence, which becomes dominant at higher frequencies. The measured frequency noise spectrum can thus be modeled as [43,44]

$$S_{f_i}(f) = S_0 f^0 + S_1 f^{-1} + S_2 f^{-2} + S_3 f^2. \quad (2)$$

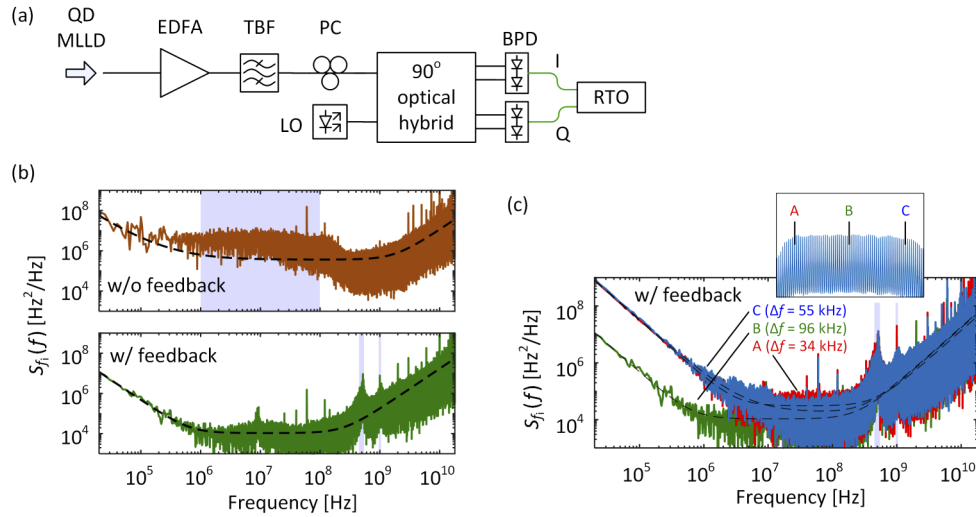


**Fig. 2.** Phase-noise characterization of QD-MLLD with and without optical feedback. (a) Experimental setup. A tunable narrow band-pass filter (TBF) is used to select distinct tones from the comb. A polarization controller (PC) at the input of a  $90^\circ$  optical hybrid is used to match the polarization of the selected tone to that of the narrowband local-oscillator (LO) tone at the input of the hybrid. Balanced photodetectors (BPD) are used to extract the in-phase (I) and the quadrature (Q) component of the beat note. The electrical signals are sampled by a real-time oscilloscope (RTO) for offline processing. (b) Measured FM-noise spectra of a QD-MLLD tone (designated as B in Fig. 2(c)) without (upper plot) and with external-cavity feedback (lower plot). The dashed lines indicate the model fit to the measured frequency noise spectrum according to Eq. (2). In these fits, the measurement data within the grey shaded areas was ignored since it is not represented by the rather simple model of Eq. (2). The fits reveal intrinsic linewidths of 1.1 MHz for the free-running QD-MLLD without feedback, and of 34 kHz for the device with optical feedback. (c) Measured FM-noise spectra of three tones of a QD-MLLD with feedback. The inset indicates the relative location of the respective comb tones inside the comb spectrum. The intrinsic linewidths amount to  $\Delta f_A = 96$  kHz,  $\Delta f_B = 34$  kHz, and  $\Delta f_C = 55$  kHz, respectively. Hence, despite the typical increase of the intrinsic linewidths of the tones towards the edge of the comb [40,41], the external-cavity feedback can greatly reduce the frequency noise throughout the comb spectrum when compared to the FM noise without external feedback.

The coefficients  $S_0 \dots S_3$  quantify the different frequency noise contributions. The intrinsic (short-term) Lorentzian linewidth  $\Delta f$  of a laser can be estimated from the white frequency-noise level as  $\Delta f = \pi S_0$ .

Figure 2(b), upper plot depicts the frequency-noise spectrum of a QD-MLLD comb tone without external-cavity feedback. The dashed line indicates the model fit to the measured frequency noise spectrum according to Eq. (2). The measured noise spectrum in the range 1...100 MHz (shaded in grey) is not considered when performing the fit – the enhanced frequency noise in this region is attributed to relaxation oscillations of the carrier density in the QD gain section, which are not contained in the rather simple model according to Eq. (2) [43,45,46]. Including this effect would introduce at least three additional free parameters related to the damping and the resonance frequency of the relaxation oscillation as well as to the linewidth enhancement factor ( $\alpha$ -factor) of the laser to properly describe the Schawlow-Townes-Henry frequency noise [47]. Fitting Eq. (2) to the remaining regions of the measured frequency noise spectrum leads to  $S_0 = 3.6 \times 10^5$  Hz,  $S_1 = 2.5 \times 10^{11}$  Hz<sup>2</sup>,  $S_2 = 1.7 \times 10^{16}$  Hz<sup>3</sup>, and

$S_3 = 1.1 \times 10^{-13} \text{ Hz}^{-1}$ . The estimated white frequency-noise level corresponds to an intrinsic linewidth of about  $\Delta f = \pi S_0 = (1.1 \pm 0.2) \text{ MHz}$  for this comb tone, where the specified uncertainty refers to the 95% confidence interval. Note that the omission of the frequency range 1 . . . 100 MHz in the fit should still lead to a reliable prediction of the data transmission performance: Frequency-noise components below 100 MHz are usually anyway compensated by phase tracking, whereas spectral components above 100 MHz can lead to degradation of the signal quality [16]. The lower plot in Fig. 2(b) depicts the frequency-noise spectrum of the same QD-MLLD comb tone under the influence of external-cavity feedback. The dashed line indicates again the model fit of the measured frequency noise spectrum according to Eq. (2). Also here, the relatively broadband noise peaks in the ranges 450 . . . 550 MHz and 0.95 . . . 1.05 GHz. These ranges are not considered when performing the fit – we attribute the peaks to side modes of the comb tone induced by the external-cavity feedback which are not contained in the model leading to Eq. (2). Note these noise peaks may be avoided by using dual-cavity resonant feedback [36]. The fit leads to  $S_0 = 1.1 \times 10^4 \text{ Hz}$ ,  $S_2 = 4.7 \times 10^{14} \text{ Hz}^3$ ,  $S_3 = 1.7 \times 10^{-13} \text{ Hz}^{-1}$ , and a negligible  $S_1$ . The estimated white frequency-noise level corresponds to an intrinsic linewidth of  $\Delta f = (34 \pm 10) \text{ kHz}$ , corresponding to a reduction of approximately two orders of magnitude as compared to the case without external-cavity feedback. This is in good agreement with other reported results [29,33].

To investigate the effect of optical feedback on the optical properties of different comb lines, we evaluated the frequency noise spectra of three widely separated tones of the comb, see Fig. 2(c). The dashed lines indicate again the model fits to the measured spectra according to Eq. (2). The relative locations of the comb tones within the comb spectrum are indicated in the inset. Comb line B corresponds to the results presented in Fig. 2(b) with an intrinsic linewidth of  $\Delta f_B = 34 \text{ kHz}$ . For the comb lines A and C, we find intrinsic linewidths of  $\Delta f_A = 96 \text{ kHz}$  and  $\Delta f_C = 55 \text{ kHz}$ , respectively. Hence, despite the typical increase of the intrinsic linewidths of the tones towards the edge of the comb [40,41], the external-cavity feedback can greatly reduce the frequency noise throughout the comb spectrum when compared to the frequency noise without external feedback. Note that, due to the presence of flicker ( $\propto f^{-1}$ ) and random-walk ( $\propto f^{-2}$ ) frequency noise, the intrinsic optical linewidths of the various tones are not any more directly connected to the RF linewidth [48], since the underlying relations derived in [41] are only valid under the assumption that all linewidths are dominated by the spectrally white ( $f^0$ ) component.

### 3. WDM transmission over 75 km at a net data rate of 11.215 Tbit/s using 32QAM

To demonstrate that feedback-stabilized QD-MLLD are well suited as multi-wavelength light sources for high-speed communications with higher-order modulation formats, we perform WDM experiments using 32-state quadrature amplitude modulation (32QAM). The experimental setup is shown in Fig. 3(a). An erbium-doped fiber amplifier (EDFA1) is used to boost the total power of the QD-MLLD comb from approximately 8 dBm to approximately 17 dBm. A total number of 60 carriers out of the full QD-MLLD comb are then selected, 55 of which lie within the 3 dB bandwidth of the comb while an additional 5 carriers are within the 4 dB bandwidth. The comb is spectrally flattened by a programmable filter (PF). WDM is emulated by encoding different data in neighboring “odd” and “even” channels. To this end, we de-interleave the frequency comb lines (FSR  $\approx 25 \text{ GHz}$ ) into odd and even tones using the programmable filter (PF). Since at this FSR, the PF has a rather low extinction of approximately 20 dB, we use a 25 GHz-to-50 GHz de-interleaver (De-int.) as a second filtering element. This leads to an extinction of the unwanted tones by more than 45 dB, see power spectrum P1 in Fig. 3(b) that shows the odd and even carriers combined in one graph. The odd and the even carriers are separately amplified by EDFA2 and EDFA3 and independently modulated with data of pseudo-random binary sequences (PRBS), which are mapped to 32QAM symbols at a rate of 20 GBd. We chose a PRBS length of  $2^{11}-1$ , dictated by limitations of the memory size and the memory granularity of the arbitrary-waveform

generator (AWG) that was used to generate the data signals. In previous experiments [14], that relied on the same equipment but were performed at slightly different ratios of symbol rate and sample rate, we have verified that the performance of our system does not change if we use longer PRBS length such as  $2^{15}-1$ . We use pulses having raised-cosine power spectra with a 20% roll-off. After modulation, odd and even channels are combined, and polarization division multiplexing (PDM) is emulated by a split-delay-combine method [49]. The data stream is amplified and transmitted over 75 km of standard single-mode fiber (SSMF), see lower power spectrum P2 in Fig. 3(b). For avoiding nonlinearities, we limit the total power entering the fiber to 10 dBm.

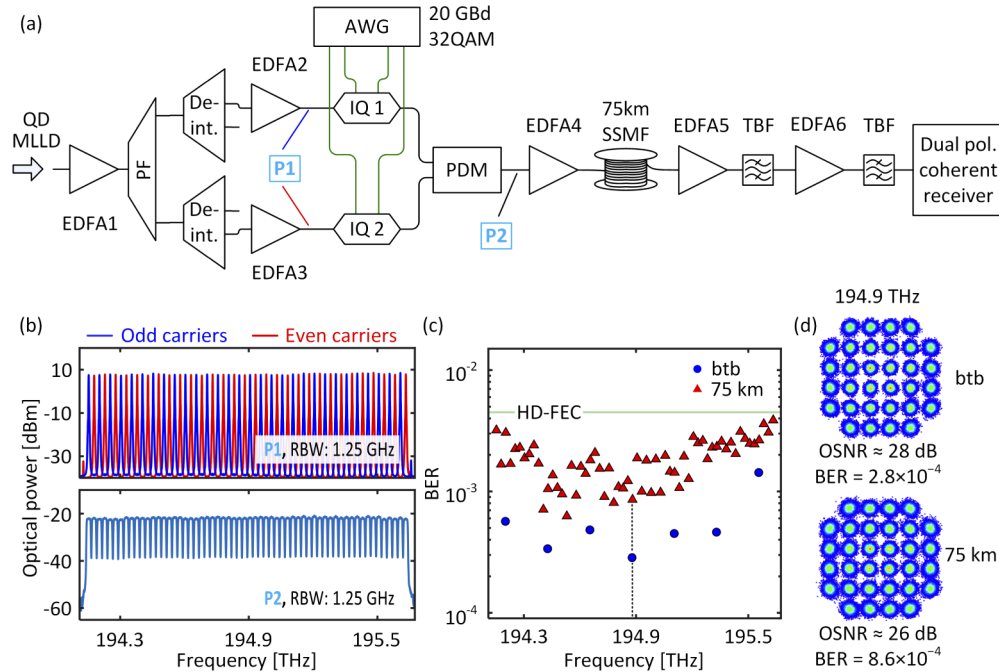


**Fig. 3.** WDM transmission experiment using a feedback-stabilized QD-MLLD comb according to Fig. 1(b). (a) Setup for the WDM experiment. An erbium-doped fiber amplifier (EDFA1) boosts the total power of the QD-MLLD comb to approximately 17 dBm, and a total of 60 carriers are then selected and spectrally flattened by a programmable filter (PF). The PF is also used to de-interleave the frequency comb lines (FSR  $\approx$  25 GHz) into odd and even tones for emulating WDM transmission by encoding different data in neighboring channels. In addition, we use a 25 GHz-to-50 GHz de-interleaver (De-int.) as a second filter element to further increase the extinction of the unwanted tones. Both the odd and the even carriers are amplified by subsequent EDFA2 and EDFA3 and independently modulated with 32QAM symbols at a rate of 20 GBd. We use pulses having raised-cosine power spectra with a 20% roll-off. After modulation, odd and even channels are combined, and polarization division multiplexing (PDM) is emulated by a split-delay-combine method. The data stream is amplified and transmitted over 75 km of standard single-mode fiber (SSMF). (b) Combined spectra of both odd and even carriers taken at position P1, i.e., before modulation (top) and spectrum of 60 modulated channels measured at position P2 (bottom). (c) BER of the transmitted channels for both back-to-back (btb) and 75 km fiber transmission. (d) Example constellation diagrams of the channel at 194.9 THz (indicated by the vertical dashed line) for btb and 75 km fiber transmission. TBF: tunable band pass filter.

At the receiver, we employ a two-stage amplification scheme using a first fiber amplifier (EDFA5) for boosting the WDM signal as a whole, then selecting the channel of interest with a tunable bandpass filter (TBF) for amplification with a second amplifier (EDFA6), followed by another tunable band pass filter (passband 1.5 nm) to suppress out-of-band amplified spontaneous emission (ASE). At the input of EDFA6, the power of the selected WDM channels varies between  $-19$  dBm and  $-16$  dBm, depending on the spectral position of the channel. Given the flat spectrum of the transmitted WDM signal, Fig. 3(b), we attribute these variations to the slightly wavelength-dependent gain of EDFA4 and EDFA5. Note, however, that EDFA6 is operated in constant-output-power mode, such that the power levels at the input of the coherent receiver do not vary significantly from channel to channel. The selected channel is then received with an optical modulation analyzer (OMA, Keysight N4391A), and processed using Keysight's vector signal analyzer (VSA) software. The VSA processing comprises spectral filtering, blind Stokes-space polarization demultiplexing [50], chromatic dispersion compensation, and a 55-tap adaptive blind equalizer based on the decision-directed least-mean-squares (LMS) algorithm. Carrier phase estimation is done through a block-wise Viterbi & Viterbi algorithm with a block length of 1024 symbols [51]. We also measured the optical signal-to-noise power ratio (OSNR) of our WDM channels at the receiver. To this end, we had to rely on the received electrical signal, since the channel separation was too small for a reliable measurement with an optical spectrum analyzer. We found OSNR values in the range of 23 . . . 26 dB, defined with respect to the usual reference noise bandwidth of 0.1 nm.

Figure 3(c) depicts the extracted bit error ratios (BER) for fiber transmission of all channels along with the back-to-back (btb) BER for seven randomly selected channels. When transmitting over a 75 km-long SSMF, all BER values are below  $4.0 \times 10^{-3}$  with a 95% confidence level [52] and are hence compatible with the threshold of  $4.45 \times 10^{-3}$  for forward error correction (FEC) with 7% overhead [53]. This leads to a line rate (net data rate) of 12 Tbit/s (11.215 Tbit/s) with a net spectral efficiency (SE) of 7.5 bit/s/Hz after deduction of FEC overhead. Note that this SE is significantly below the 10 bit/s/Hz that could be theoretically achieved by dual-polarization 32QAM signaling. The reduced SE is a direct consequence of the rather high roll-off of 20% that was chosen deliberately to avoid problems with the clock recovery in the VSA software. Using a more robust clock-recovery technique would allow to reduce the roll-off and thus to increase the SE. Example constellation diagrams of the comb line at carrier frequency 194.9 THz for both back-to-back and 75 km fiber transmission are shown in Fig. 3(d) along with the corresponding OSNR and BER values. The back-to-back experiment exhibits higher OSNR than the transmission experiment and performs better in terms of BER. We thus believe that the signal quality in our transmission experiments is limited by OSNR and that phase noise of the optical carrier does not play a role once stabilization by external-cavity feedback is used. This is in line with the fact that the constellation points in Fig. 3(d) have an approximately symmetric circular spread. A closer observation of the back-to-back constellation diagram may also reveal the impact of relative intensity noise (RIN), which leads to a scattering of the constellation points that is most pronounced for the outer symbols. Therefore, the relatively high RIN of QD-MLLD could still be a limitation at high OSNR values, even if external-cavity feedback is employed, see Appendix A for a RIN characterization of the QD-MLLD with and without external-cavity feedback. We also tried 20GBd 32QAM-transmission without external-cavity feedback but could not recover the signal at the receiver because of excessive phase noise. To the best of our knowledge, these experiments represent the first demonstration of 32QAM transmission using a QD-MLLD as a multi-wavelength light source, leading to the highest spectral efficiency reported for such a device. The line rate of 12 Tbit/s and the transmission distance of 75 km is on par with the 11.55 Tbit/s and the 75 km achieved by using native QD-MLLD with advanced phase tracking [16] and compares well with the 12.032 Tbit/s that were demonstrated for 16QAM back-to-back signaling with feedback-stabilized quantum-dot MLLD for 16QAM [23].



#### 4. Extension to higher symbol rates

In our experiments, we used rather low symbol rates of 20 GBd because we had access to QD-MLLD chips only with an FSR of approximately 25 GHz. In addition, this choice allows us to better isolate the impact of phase noise, exploiting the fact that signals with lower symbol are more prone to phase noise and less sensitive to ASE noise. Clearly, the reduced phase noise should also improve the transmission performance at higher symbol rates beyond 50 GBd that are expected to become the standard in coherent transmission [54,55]. Note that, with OCNR values in excess of 37 dB and comb line powers in excess of  $-10$  dBm as indicated in Fig. 1(c), QD-MLLD should support link-limited transmission of up to 56 GBd 64QAM (600 Gbit/s) per line over more than 10 fiber spans of 75 km each, i.e., for a reach of  $> 700$  km [2]. To investigate the transmission performance of QD-MLLD in such scenarios, we performed Matlab simulations using the measured phase-noise characteristics of our QD-MLLD along with different levels of AWGN, quantified by the OSNR. To this end, we first extract time series of random phase fluctuations from the phase-noise measurements presented in Fig. 2(b). Note that the measured phase-noise time series is also impacted by the ASE of the EDFA in the measurement setup, see Fig. 2(a). This leads to an  $f^2$ - component in the corresponding frequency-noise spectrum, Fig. 2(b), which we suppress by applying a first-order low-pass filter with amplitude transfer function  $1/(1 + j(f/f_{3dB}))$  to the measured frequency-noise time series, where the cut-off  $f_{3dB} = \sqrt{S_0/S_3}$  is defined by the frequency for which the  $f^2$ - component starts to dominate the power spectral density of the frequency noise. Figure 4(a) shows the measured frequency-noise spectrum of a tone (tone B in Fig. 2(c)) extracted from a free-running QD-MLLD (black) and the corresponding model fit according to Eq. (2) (black/white dotted) along with the filtered power spectrum (blue) and the model fit without the  $f^2$ - component (blue/white dotted). Figure 4(b) shows the corresponding quantities for the same tone extracted from the feedback-stabilized device. The corresponding time series  $\phi_c(t)$  of the carrier phase fluctuations is obtained by integrating the time series of the frequency-noise over time.

The time series  $\phi_c(t)$  of the carrier phase fluctuations is then used in the Matlab simulation, which is schematically illustrated in Fig. 4(c). In a first step, a PRBS is mapped to a 64QAM symbol pattern with one sample per symbol in the modulator. The carrier phase noise is then emulated by resampling the time series  $\phi_c(t)$  at the symbol rate and by adding the fluctuations to the phase of the modulated symbols using phasor multiplication. AWGN is added to the resulting modulated signal to emulate different OSNR levels at the receiver. The OSNR is specified with respect to the usual reference bandwidth of 0.1 nm (12.5 GHz). In our transmission scenario, we assume that the LO tone at the coherent receiver is also derived from a QD-MLLD that is nominally identical to the device at the transmitter. This is emulated by adding a time series of LO phase fluctuations  $\phi_{LO}(t)$  to the phases of the data signal prior to reception. For simplicity, we derive the time series  $\phi_{LO}(t)$  from a previously unused section of the measured carrier phase fluctuations  $\phi_c(t)$ , i.e.,  $\phi_{LO}(t) = \phi_c(t - \tau_d)$ , where the delay  $\tau_d$  is chosen much larger than the inverse of the intrinsic linewidth to ensure statistically independent phase-noise processes. The received signals are then demodulated by employing two different phase-estimation techniques: Symbol-wise blind phase search (BPS) with 45 test angles [16,56] and numerically much simpler Viterbi-Viterbi (VV) processing with fourth-power phase estimation [57,58]. Other processing steps that are usually employed in conventional coherent receivers, e.g., for polarization demultiplexing or equalization, are not relevant here as these effects are not included in the rather simple AWGN channel model.

Figure 4(d) and (e) show the BER obtained by BPS and VV at symbol rates of 20 GBd and 56 GBd at different OSNR levels with and without phase-noise suppression by external-cavity feedback. For BPS, we use an averaging block length between 8 and 64 symbols, which is optimized individually for each OSNR value. For both 20 GBd and 56 GBd, the BER obtained for the feedback-stabilized QD-MLLD ('w/ feedback', red) is close to the theoretical values

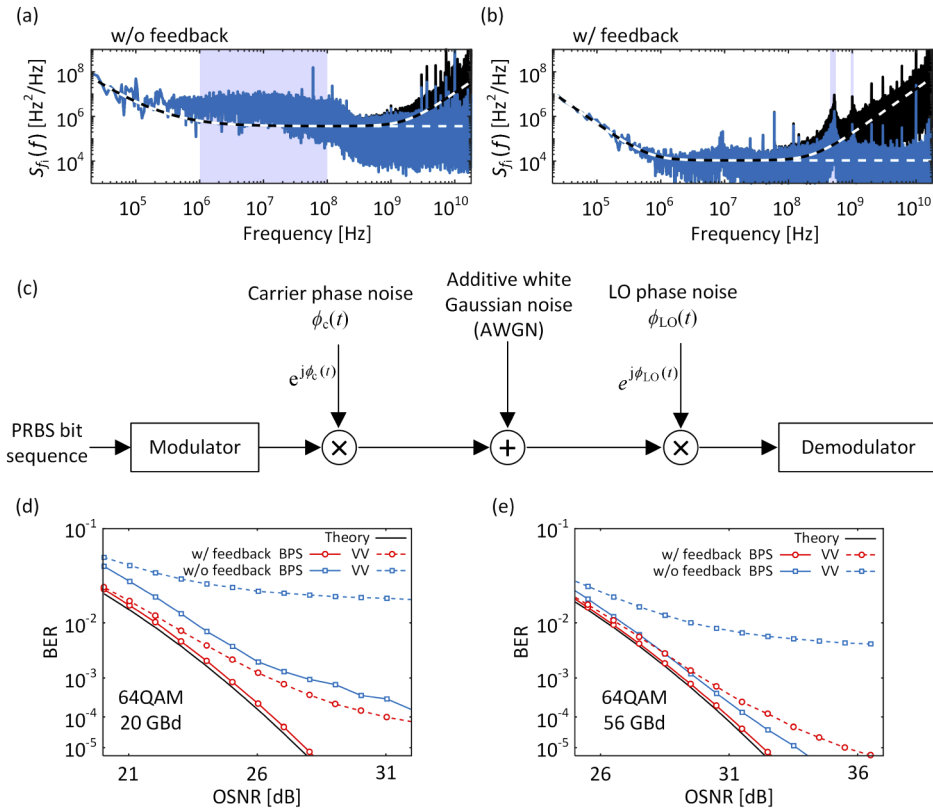


**Fig. 4.** Simulation of 64QAM transmission performance of feedback-stabilized and free-running QD-MLLD. (a, b) Measured frequency-noise spectra (black) for QD-MLLD without (w/o) and with (w/) external-cavity feedback, respectively, along with filtered counterparts (blue) that are used to emulate the phase noise of the carrier and the LO tone in the transmission simulation. The filtering is used to suppress the unwanted impact of ASE noise ( $\sim f^2$ ) in the phase-noise measurement. The dashed lines correspond to the respective model fits according to Eq. (2), see also Fig. 2(b). (c) Simulation setup. A PRBS bit sequence is mapped to a 64QAM symbol pattern with one sample per symbol in the modulator. Measured phase data is added to the phase of the modulated symbols using phasor multiplication to emulate the carrier phase noise  $\phi_c(t)$  and the LO-tone phase noise  $\phi_{LO}(t)$ . AWGN is added to the resulting modulated signal to emulate different optical signal-to-noise power ratios (OSNR) at the receiver. The received signal is then demodulated by employing the blind phase search (BPS) algorithm for carrier recovery [16,56]. (d, e) Simulated bit error rates (BER) as a function of OSNR for 64QAM signaling at symbol rates of 20 GBd and 56 GBd, respectively. We use highly effective symbol-wise blind phase search (BPS) with 45 test angles and numerically much simpler Viterbi-Viterbi (VV) processing with fourth-power phase estimation. For BPS, the BER obtained for the feedback-stabilized QD-MLLD ('w/ feedback', red) is close to the theoretical values ('Theory', blue) that are estimated only based on the OSNR, without any phase noise at all. In contrast to that, the free-running QD-MLLD ('w/o feedback', blue) performs worse. A clear performance advantage is found even for the higher symbol rate of 56 GBd, which should be much less prone to phase noise than the 20 GBd transmission. For the numerically less complex VV algorithm, the benefit of phase-noise reduction by external-cavity feedback becomes even more prominent, indicating that feedback stabilization of QD-MLLD may also allow to simplify digital phase estimation.

(‘Theory’, blue) that are estimated only based on the OSNR, without considering phase noise at all. We hence conclude that, for feedback-stabilized QD-MLLD and practically relevant OSNR levels at the receiver, the transmission performance obtained with BPS is limited by OSNR rather than by phase noise, and that the peaks that occur in the frequency-noise spectra of Fig. 2(b) and 4(b) do not represent a relevant limitation. In contrast to that, the free-running QD-MLLD (‘w/o feedback’, blue) performs worse. As expected, the positive impact of phase-noise reduction is more pronounced at the lower symbol rate of 20 GBd than at 56 GBd. The benefit of phase-noise reduction by external-cavity feedback becomes even more prominent when using simpler phase estimation techniques such as VV. Also, here we adapt the block individually for each OSNR value. Within the considered range of OSNR, the BER achieved with VV and a free-running QD-MLLD exceeds the threshold of  $4.45 \times 10^{-3}$  for FEC with 7% overhead [53], even for a symbol rate of 56 GBd, but improves drastically once feedback stabilization is used. We hence conclude that feedback stabilization of QD-MLLD offers a clear performance advantage for a wide range of technically relevant OSNR levels and may even allow to reduce the complexity of the phase estimation algorithm.

## 5. Summary and outlook

We demonstrate that QD-MLLD with coherent external feedback can be used for spectrally efficient high-speed data transmission using advanced modulation formats beyond 16QAM. In our experiment, we use 32QAM signaling on 60 carriers to for data transmission at a line rate of 12 Tbit/s (net data rate 11.215 Tbit/s) over a 75 km-long standard single mode fiber link at a spectral efficiency of 7.5 bit/s/Hz. To the best of our knowledge, this is the first time that an optical frequency comb from a QD-MLLD has been used for data transmission with 32QAM as a modulation format. We also show by simulations that external-cavity feedback should give clear performance advantages for 64QAM signaling and symbol rates of, e.g., 56 GBd. For real-world systems, the free-space external cavity may be replaced by integrated optical feedback circuits that rely, e.g., on ring resonators [24]. The requirements with respect to the quality of these resonators are relatively low – significant linewidth reductions may already be achieved with external-cavity round-trip losses of more than 20 dB [32]. Established ring-resonator technologies [59,60] should allow to easily fulfill these requirements, thereby opening a route towards chip-scale WDM transceivers that exploit feedback-stabilized QD-MLLD to support line rates of tens of Tbit/s.

## Appendix A: Relative intensity noise (RIN) of QD-MLLD with and without external-cavity feedback

From the beat signals recorded for the optical linewidth measurements, see Fig. 2(b) and (c), we also extracted the associated relative intensity noise (RIN) of individual comb tones. The results are shown in Fig. 5. For free-running QD-MLLD without external-cavity feedback, we find RIN levels of approximately  $-115 \text{ dB Hz}^{-1}$  for frequencies below 1 GHz, which is well in line with other experiments [61,62]. Under the influence of external-cavity feedback, the RIN spectrum experiences a modulation that corresponds to the free spectral range of the 300 mm-long external cavity. The overall RIN level, however, remains unchanged. Note that the sensitivity of the RIN measurement is limited to a minimum detectable level of approximately  $-127 \text{ dB Hz}^{-1}$  due to the ASE noise of the EDFA that was used in the signal path when measuring the beat note, see Fig. 2(a) in Section 2.

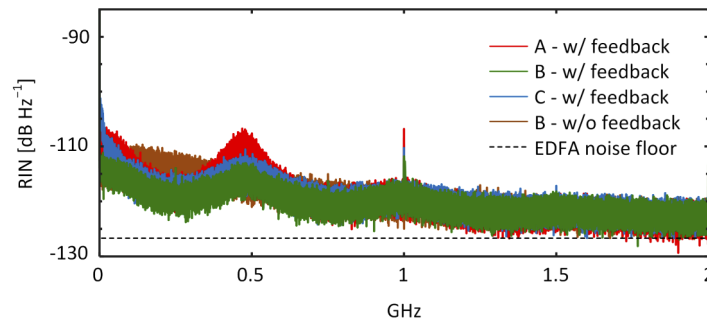


**Fig. 5.** Relative intensity noise (RIN) spectra extracted from the beat notes of the linewidth measurement. We find that external-cavity feedback leads to a spectral modulation of the RIN according to the free spectral range of the 300 mm-long external cavity, while leaving the overall RIN level unchanged. Due to an EDFA that was used in the signal path signal path when measuring the beat notes, sensitivity of the RIN measurement is limited to a noise floor of approximately  $-127 \text{ dB Hz}^{-1}$ .

## Funding

H2020 research and innovation programme ‘MICROCOMB’ (812818); H2020 research and innovation programme ‘TeraSlice’ (863322); European Research Council (773248); Seventh Framework Programme (619591); Deutsche Forschungsgemeinschaft (CRC 1173, project B3); Alfried Krupp von Bohlen und Halbach-Stiftung; Helmholtz International Research School for Teratronics, Karlsruher Institut für Technologie; Erasmus Mundus Joint Doctorate program Europhotonics (159224-1-2009-1-FR-ERA MUNDUS-EMJD).

## Disclosures

The authors declare no conflicts of interest.

## References

1. Cisco White Paper, “Annual internet report, 2018–2023” (CISCO, 2020). <https://www.cisco.com/c/en/us/solutions/collateral/executive-perspectives/annual-internet-report/white-paper-c11-741490.html>.
2. P. Marin-Palomo, J. N. Kemal, T. J. Kippenberg, W. Freude, S. Randel, and C. Koos, “Performance of chip-scale optical frequency comb generators in coherent WDM communications,” *Opt. Express* **28**(9), 12897–12910 (2020).
3. V. Torres-Company, J. Schroder, A. Fulop, M. Mazur, L. Lundberg, O. B. Helgason, M. Karlsson, and P. A. Andrekson, “Laser frequency combs for coherent optical communications,” *J. Lightwave Technol.* **37**(7), 1663–1670 (2019).
4. P. Marin-Palomo, J. N. Kemal, M. Karpov, A. Kordts, J. Pfeifle, M. H. P. Pfeiffer, P. Trocha, S. Wolf, V. Brasch, M. H. Anderson, R. Rosenberger, K. Vijayan, W. Freude, T. J. Kippenberg, and C. Koos, “Microresonator-based solitons for massively parallel coherent optical communications,” *Nature* **546**(7657), 274–279 (2017).
5. A. Fülöp, M. Mazur, A. Lorences-Riesgo, Ó. B. Helgason, P.-H. Wang, Y. Xuan, D. E. Leaird, M. Qi, P. A. Andrekson, A. M. Weiner, and V. Torres-Company, “High-order coherent communications using mode-locked dark-pulse Kerr combs from microresonators,” *Nat. Commun.* **9**(1), 1598 (2018).
6. H. Hu, F. Da Ros, M. Pu, F. Ye, K. Ingerslev, E. Porto da Silva, M. Nooruzzaman, Y. Amma, Y. Sasaki, T. Mizuno, Y. Miyamoto, L. Ottaviano, E. Semenova, P. Guan, D. Zibar, M. Galili, K. Yvind, T. Morioka, and L. K. Oxenløwe, “Single-source chip-based frequency comb enabling extreme parallel data transmission,” *Nat. Photonics* **12**(8), 469–473 (2018).
7. J. Pfeifle, V. Vujicic, R. T. Watts, P. C. Schindler, C. Weimann, R. Zhou, W. Freude, L. P. Barry, and C. Koos, “Flexible terabit/s Nyquist-WDM super-channels using a gain-switched comb source,” *Opt. Express* **23**(2), 724–738 (2015).
8. C. Weimann, P. C. Schindler, R. Palmer, S. Wolf, D. Bekele, D. Korn, J. Pfeifle, S. Koeber, R. Schmogrow, L. Alloatti, D. Elder, H. Yu, W. Bogaerts, L. R. Dalton, W. Freude, J. Leuthold, and C. Koos, “Silicon-organic hybrid (SOH) frequency comb sources for terabit/s data transmission,” *Opt. Express* **22**(3), 3629–3637 (2014).
9. J. Lin, H. Sepeshian, Y. Xu, L. A. Rusch, and W. Shi, “Frequency comb generation using a CMOS compatible SiP DD-MZM for flexible networks,” *IEEE Photonics Technol. Lett.* **30**(17), 1495–1498 (2018).

10. V. Vujcic, A. Anthur, V. Panapakkam, R. Zhou, Q. Gaimard, K. Merghem, F. Lelarge, A. Ramdane, and L. P. Barry, "Tbit/s optical interconnects based on low linewidth quantum-dash lasers and coherent detection," in *Conference on Lasers and Electro-Optics* (Optical Society of America, 2016), paper SF2F.4.
11. P. J. Delfyett, S. Gee, M. T. Choi, H. Izadpanah, W. Lee, S. Ozharar, F. Quinlan, and T. Yilmaz, "Optical frequency combs from semiconductor lasers and applications in ultrawideband signal processing and communications," *J. Lightwave Technol.* **24**(7), 2701–2719 (2006).
12. N. K. Fontaine, R. P. Scott, L. Zhou, F. M. Soares, J. P. Heritage, and S. J. B. Yoo, "Real-time full-field arbitrary optical waveform measurement," *Nat. Photonics* **4**(4), 248–254 (2010).
13. J. N. Kemal, J. Pfeifle, P. Marin-Palomo, M. D. G. Pascual, S. Wolf, F. Smyth, W. Freude, and C. Koos, "Multi-wavelength coherent transmission using an optical frequency comb as a local oscillator," *Opt. Express* **24**(22), 25432–22445 (2016).
14. J. N. Kemal, P. Marin-Palomo, V. Panapakkam, P. Trocha, S. Wolf, K. Merghem, F. Lelarge, A. Ramdane, S. Randel, W. Freude, and C. Koos, "Coherent WDM transmission using quantum-dash mode-locked laser diodes as multi-wavelength source and local oscillator," *Opt. Express* **27**(22), 31164–31175 (2019).
15. J. Pfeifle, R. Watts, I. Shkarban, S. Wolf, V. Vujcic, P. Landais, N. Chimot, S. Joshi, K. Merghem, C. Calò, M. Weber, A. Ramdane, F. Lelarge, L. Barry, W. Freude, and C. Koos, "Simultaneous Phase Noise Reduction of 30 Comb Lines from a Quantum-Dash Mode-Locked Laser Diode Enabling Coherent Tbit/s Data Transmission," in *Optical Fiber Communication Conference* (Optical Society of America, 2015), paper Tu3I.5.
16. P. Marin-Palomo, J. N. Kemal, P. Trocha, S. Wolf, K. Merghem, F. Lelarge, A. Ramdane, W. Freude, S. Randel, and C. Koos, "Comb-based WDM transmission at 10 Tbit/s using a DC-driven quantum-dash mode-locked laser diode," *Opt. Express* **27**(22), 31110–31129 (2019).
17. F. Lelarge, B. Dagens, J. Renaudier, R. Brenot, A. Accard, F. van Dijk, D. Make, O. Le Gouezigou, J.-G. Provost, F. Poingt, J. Landreau, O. Drisse, E. Derouin, B. Rousseau, F. Pommereau, and G.-H. Duan, "Recent advances on InAs/InP quantum dash based semiconductor basers and optical amplifiers operating at 1.55  $\mu\text{m}$ ," *IEEE J. Sel. Top. Quantum Electron.* **13**(1), 111–124 (2007).
18. Z. G. Lu, J. R. Liu, S. Raymond, P. J. Poole, P. J. Barrios, and D. Poitras, "312-fs pulse generation from a passive C-band InAs/InP quantum dot mode-locked laser," *Opt. Express* **16**(14), 10835 (2008).
19. G. Liu, Z. Lu, J. Liu, Y. Mao, M. Vachon, C. Song, and P. J. Poole, "A passively mode-locked quantum dot laser with 10.8 Tbit/s transmission over 100-km SSMF," in *Optical Fiber Communication Conference* (Optical Society of America, 2020), paper W2A.2.
20. A. Akrouf, A. Shen, R. Brenot, F. Van Dijk, O. Legouezigou, F. Pommereau, F. Lelarge, A. Ramdane, and G.-H. Duan, "Separate Error-Free Transmission of Eight Channels at 10 Gb/s Using Comb Generation in a Quantum-Dash-Based Mode-Locked Laser," *IEEE Photonics Technol. Lett.* **21**(23), 1746–1748 (2009).
21. C. Calò, V. Vujcic, R. Watts, C. Browning, K. Merghem, V. Panapakkam, F. Lelarge, A. Martinez, B.-E. Benkelfat, A. Ramdane, and L. P. Barry, "Single-section quantum well mode-locked laser for 400 Gb/s SSB-OFDM transmission," *Opt. Express* **23**(20), 26442 (2015).
22. J. N. Kemal, P. Marin-Palomo, K. Merghem, G. Aubin, C. Calò, R. Brenot, F. Lelarge, A. Ramdane, S. Randel, W. Freude, and C. Koos, "32QAM WDM transmission using a quantum-dash passively mode-locked Laser with resonant feedback," in *Optical Fiber Communication Conference Postdeadline Papers* (Optical Society of America, 2017), paper Th5C.3.
23. Z. Lu, J. Liu, L. Mao, C.-Y. Song, J. Weber, and P. Poole, "12.032 Tbit/s coherent transmission using an ultra-narrow linewidth quantum dot 34.46-GHz C-Band coherent comb laser," in *Next-Generation Optical Communication: Components, Sub-Systems, and Systems VIII*, G. Li and X. Zhou, eds. (SPIE, 2019), p. 23.
24. J. Hauck, A. Zazzi, A. Garreau, F. Lelarge, A. Moscoso-Martir, F. Merget, and J. Witzens, "Semiconductor laser mode locking stabilization with optical feedback from a silicon PIC," *J. Lightwave Technol.* **37**(14), 3483–3494 (2019).
25. C. Xing and E. A. Avrutin, "Multimode spectra and active mode locking potential of quantum dot lasers," *J. Appl. Phys.* **97**(10), 104301 (2005).
26. R. Rosales, K. Merghem, A. Martinez, A. Akrouf, J.-P. Tournenc, A. Accard, F. Lelarge, and A. Ramdane, "InAs/InP quantum-dot passively mode-locked lasers for 1.55- $\mu\text{m}$  applications," *IEEE J. Sel. Top. Quantum Electron.* **17**(5), 1292–1301 (2011).
27. D. Auth, L. Drzewietzki, C. Weber, A. Klehr, A. Knigge, and S. Breuer, "Repetition rate control of optical Self-Injected passively mode-locked quantum-well Lasers: Experiment and simulation," *Electron. Lett.* **54**(6), 374–376 (2018).
28. D. Arsenijević, M. Kleinert, and D. Bimberg, "Phase noise and jitter reduction by optical feedback on passively mode-locked quantum-dot lasers," *Appl. Phys. Lett.* **103**(23), 231101 (2013).
29. Z. G. Lu, J. R. Liu, P. J. Poole, C. Y. Song, and S. D. Chang, "Ultra-narrow linewidth quantum dot coherent comb lasers with self-injection feedback locking," *Opt. Express* **26**(9), 11909–11914 (2018).
30. F. Grillot, C. Y. Lin, N. A. Naderi, M. Pochet, and L. F. Lester, "Optical feedback instabilities in a monolithic InAs/GaAs quantum dot passively mode-locked laser," *Appl. Phys. Lett.* **94**(15), 153503 (2009).
31. E. A. Avrutin, S. Xibin, and B. M. Russell, "Optical feedback tolerance of mode-locked laser diodes and some feedback reduction methods: a numerical investigation," *Opt. Quantum Electron.* **40**(14-15), 1175–1180 (2008).
32. H. Asghar, W. Wei, P. Kumar, E. Sooudi, and J. G. McInerney, "Stabilization of self-mode-locked quantum dash lasers by symmetric dual-loop optical feedback," *Opt. Express* **26**(4), 4581–4592 (2018).

33. K. Merghem, V. Panapakkam, Q. Gaimard, F. Lelarge, and A. Ramdane, "Narrow linewidth frequency comb source based on self-injected quantum-dash passively mode-locked laser," in *Conference on Lasers and Electro-Optics* (Optical Society of America, 2017), paper SW1C.5.
34. E. Sooudi, G. Huyet, J. G. McInerney, F. Lelarge, K. Merghem, R. Rosales, A. Martinez, A. Ramdane, and S. P. Hegarty, "Injection-locking properties of InAs/InP-based mode-locked quantum-dash lasers at 21 GHz," *IEEE Photonics Technol. Lett.* **23**(20), 1544–1546 (2011).
35. E. Sooudi, S. Sygletos, A. D. Ellis, G. Huyet, J. G. McInerney, F. Lelarge, K. Merghem, R. Rosales, A. Martinez, A. Ramdane, and S. P. Hegarty, "Optical frequency comb generation using dual-mode injection-locking of quantum-dash mode-locked lasers: Properties and applications," *IEEE J. Quantum Electron.* **48**(10), 1327–1338 (2012).
36. M. Haji, L. Hou, A. E. Kelly, J. Akbar, J. H. Marsh, J. M. Arnold, and C. N. Ironside, "Ultralow 192 Hz RF linewidth optoelectronic oscillator based on the optical feedback of mode-locked laser diodes," in *Conference on Lasers and Electro-Optics* (Optical Society of America, 2012), paper CW1N.4.
37. E. A. Avrutin and B. M. Russell, "Dynamics and spectra of monolithic mode-locked laser diodes under external optical feedback," *IEEE J. Quantum Electron.* **45**(11), 1456–1464 (2009).
38. J. Osmundsen and N. Gade, "Influence of optical feedback on laser frequency spectrum and threshold conditions," *IEEE J. Quantum Electron.* **19**(3), 465–469 (1983).
39. F. Kéfélian, S. O'Donoghue, M. T. Todaro, J. G. McInerney, and G. Huyet, "RF linewidth in monolithic passively mode-locked semiconductor laser," *IEEE Photonics Technol. Lett.* **20**(16), 1405–1407 (2008).
40. T. Habruseva, S. O'Donoghue, N. Rebroya, F. Kéfélian, S. P. Hegarty, and G. Huyet, "Optical linewidth of a passively mode-locked semiconductor laser," *Opt. Lett.* **34**(21), 3307–3309 (2009).
41. R. Rosales, K. Merghem, A. Martinez, F. Lelarge, A. Accard, and A. Ramdane, "Timing jitter from the optical spectrum in semiconductor passively mode locked lasers," *Opt. Express* **20**(8), 9151–9160 (2012).
42. K. Kikuchi, "Characterization of semiconductor-laser phase noise and estimation of bit-error rate performance with low-speed offline digital coherent receivers," *Opt. Express* **20**(5), 5291–5302 (2012).
43. T. N. Huynh, L. Nguyen, and L. P. Barry, "Phase noise characterization of SGDBR lasers using phase modulation detection method with delayed self-heterodyne measurements," *J. Lightwave Technol.* **31**(8), 1300–1308 (2013).
44. A. L. Lance, W. D. Seal, and F. Labaar, "Phase Noise and AM Noise Measurements in the Frequency Domain," in *Infrared and Millimeter Waves 11*, 239–289, K. J. Button, Ed (Academic Press, 1984).
45. P. Spano, S. Piazzolla, and M. Tamburrini, "Phase noise in semiconductor lasers: A theoretical approach," *IEEE J. Quantum Electron.* **19**(7), 1195–1199 (1983).
46. K. Kikuchi and T. Okoshi, "FM- and AM-noise spectra of 1.3  $\mu\text{m}$  InGaAsP DFB lasers in 0–3 GHz range and determination of their linewidth enhancement factor  $\alpha$ ," *Electron. Lett.* **20**(25–26), 1044–1045 (1984).
47. C. H. Henry, "Theory of the Phase Noise and Power Spectrum of a Single Mode Injection Laser," *IEEE J. Quantum Electron.* **19**(9), 1391–1397 (1983).
48. T. Verolet, G. Aubin, Y. Lin, C. Browning, K. Merghem, F. Lelarge, C. Calo, A. Demalde, K. Mekhazni, E. Giacomidis, A. Shen, L. P. Barry, and A. Ramdane, "Mode locked laser phase noise reduction under optical feedback for coherent DWDM communication," *J. Lightw. Technol.* **8724**(21), Print ISSN: 0733-8724 (posted 15 June 2020, in press).
49. D. Hillerkuss, R. Schmogrow, M. Meyer, S. Wolf, M. Jordan, P. Kleinow, N. Lindenmann, P. C. Schindler, A. Melikyan, X. Yang, S. Ben-Ezra, B. Nebendahl, M. Dreschmann, J. Meyer, F. Parmigiani, P. Petropoulos, B. Resan, A. Oehler, K. Weingarten, L. Altenhain, T. Ellermeyer, M. Moeller, M. Huebner, J. Becker, C. Koos, W. Freude, and J. Leuthold, "Single-laser 32.5 Tbit/s Nyquist WDM transmission," *J. Opt. Commun. Netw.* **4**(10), 715–723 (2012).
50. B. Szafraniec, B. Nebendahl, and T. Marshall, "Polarization demultiplexing in Stokes space," *Opt. Express* **18**(17), 17928–17939 (2010).
51. R. Schmogrow, "Real-time digital signal processing for software-defined optical transmitters and receivers," Ph.D. dissertation (Karlsruhe Institute of Technology, 2014).
52. M. Jeruchim, "Techniques for Estimating the Bit Error Rate in the Simulation of Digital Communication Systems," *IEEE J. Sel. Areas Commun.* **2**(1), 153–170 (1984).
53. F. Chang, K. Onohara, and T. Mizuochi, "Forward error correction for 100 G transport networks," *IEEE Commun. Mag.* **48**(3), S48–S55 (2010).
54. OIF-Tech-Options-400G-01.0 white paper, "Technology options for 400G implementation" (OIF, 2015). <https://www.oiforum.com/documents/technology-options-for-400g-implementation/>.
55. K. Roberts, Q. Zhuge, I. Monga, S. Gareau, and C. Laperle, "Beyond 100 Gb/s: Capacity, Flexibility, and Network Optimization," *J. Opt. Commun. Netw.* **9**(4), C12–C24 (2017).
56. T. Pfau, S. Hoffmann, and R. Noe, "Hardware-efficient coherent digital receiver concept with feedforward carrier recovery for M-QAM constellations," *J. Lightwave Technol.* **27**(8), 989–999 (2009).
57. A. Viterbi, "Nonlinear estimation of PSK-modulated carrier phase with application to burst digital transmission," *IEEE Trans. Inf. Theory* **29**(4), 543–551 (1983).
58. K. Schuh, F. Buchali, W. Idler, T. A. Eriksson, L. Schmalen, W. Templ, L. Altenhain, U. Dümmler, R. Schmid, M. Möller, and K. Engenhardt, "Single carrier 1.2 Tbit/s transmission over 300 km with PM-64 QAM at 100 GBaud," in *Optical Fiber Communication Conference Postdeadline Papers* (Optical Society of America, 2017), paper. Th5B.5.
59. LIGENEC, "All-Nitride Core Technology," <https://www.ligentec.com/ligentec-an-technology/>.

60. M. H. P. Pfeiffer, A. Kordts, V. Brasch, M. Zervas, M. Geiselmann, J. D. Jost, and T. J. Kippenberg, "Photonic Damascene process for integrated high-Q microresonator based nonlinear photonics," *Optica* **3**(1), 20–25 (2016).
61. V. Panapakkam, A. P. Anthur, V. Vujicic, R. Zhou, Q. Gaimard, K. Merghem, G. Aubin, F. Lelarge, E. A. Viktorov, L. P. Barry, and A. Ramdane, "Amplitude and phase noise of frequency combs generated by single-section InAs/InP quantum-dash-based passively and actively mode-locked lasers," *IEEE J. Quantum Electron.* **52**(11), 1–7 (2016).
62. V. Vujicic, A. P. Anthur, A. Saljoghei, V. Panapakkam, R. Zhou, Q. Gaimard, K. Merghem, F. Lelarge, A. Ramdane, and L. P. Barry, "Mitigation of relative intensity noise of quantum dash mode-locked lasers for PAM4 based optical interconnects using encoding techniques," *Opt. Express* **25**(1), 20–29 (2017).